



The enhancement of droplet collision by electric charges and atmospheric electric fields

Shian Guo, Huiwen Xue

School of Physics, Peking University, Beijing, China

5 *Correspondence to:* Huiwen Xue (hxue@pku.edu.cn)

Abstract.

The effect of electric charges and atmospheric electric fields on droplet spectrum evolution is studied numerically. Collision efficiencies for droplet pair with radii from 2 to 1024 μm and charges from $-32 r^2$ to $+32 r^2$ (in unit of elementary charge, droplet radius r in unit of μm) in different strength of downwards electric fields (0, 200 and 400 V cm^{-1}) is computed. It is seen
10 that collision efficiency is increased by electric charges and fields, especially for a pair of small droplets.

The evolution of cloud droplet spectrum with different initial sizes is simulated using the stochastic collection equation. Results show that the electric effect is not notable for the cloud with the initial mean droplet radius $\bar{r}=15 \mu\text{m}$ or larger. For the cloud with the initial $\bar{r}=9 \mu\text{m}$, the electric charge without field could evidently accelerate large-drop formation compared to the uncharged condition, and the existence of electric fields further accelerates it. For the cloud with the initial $\bar{r}=6.5 \mu\text{m}$, it
15 is difficult for gravitational collision to occur, and the electric field could significantly enhance the collision process. Results of this study indicate that electric charges and fields could accelerate large-drop formation in natural conditions, particularly for clouds with small droplet size.

1 Introduction

20 Observations show that cloud droplets and aerosols carry net electric charges. Droplet charges can reach $|q| \approx 42r^2$ in the unit of elementary charge, with the droplet radius in the unit of μm (after unit conversion from Pruppacher and Klett, 1997). Vertical electric fields always exist in atmosphere. Especially in convective clouds, the electric field can reach the magnitude of 10^3V cm^{-1} . Cloud droplets (whether with or without net charge) could be regarded as spherical conductor approximately
25 (Davis, 1964). It is significant that, as conductors, droplet pairs have electrostatic induction effect. This can lead to strong attraction at very small distance, regardless of the sign of charge. Charged droplets can thus be attracted strongly at small distances.

According to Davis (1964), the force between two charged droplets in uniform electric field is well approximated as two spherical electric conductors. Though there is no explicit analytical expression for the interaction, a set of computational
30 method is given. Schlamp et al. (1976) used this method to show the effect of electric charges and atmospheric electric fields on collision efficiency, which demonstrated that the collision efficiencies between small droplets (about 1~10 μm) are



enhanced by an order of magnitude in thunderstorm condition, while collision between large droplets is hardly affected. Note that Schlamp et al. (1976) didn't simulate the spectrum evolution process.

As for the electric effect on droplet spectrum evolution, few researches have been conducted. Khain et al. (2004), focused on weather modification, showed that droplet electric charges could enhance precipitation. They considered interaction of droplet pair by image charge, and use Stokes Flow to calculate hydrodynamic interaction. The charge limit is set up to the air-breakdown limit. It is found that a small fraction of extremely charged particles could trigger the collision process, and thus accelerate raindrop formation or fog elimination significantly.

Previous studies about Albrecht (1989) effect show that increase of aerosol number decreases cloud droplet size, and thus extending cloud lifetime and suppress precipitation. But with the existence of electric charges, the Albrecht effect might be partially weakened. As mentioned above, Schlamp et al. (1976) had already shown that smaller droplets are more sensitive to electric effect. So, the coupling of electric effect and Albrecht effect needs to be considered.

This study investigates the effect of electric charges and fields on droplet collision efficiency and the evolution of droplet spectrum. Different initial droplet size spectra and different electric conditions are considered. Section 2 describes the theory of droplet collision and stochastic collection equation. Section 3 and 4 present the numerical methods. Section 5 shows the numerical results of electric effects on collision efficiency, and on cloud spectrum evolution.

2 Stochastic Collection Equation

The evolution of droplet size spectrum due to collision-coalescence is described by the stochastic collection equation (SCE), which was first proposed by Telford (1955), and is shown as (Lamb and Verlinde, 2011, p.442)

$$\frac{\partial n(m, t)}{\partial t} = \int_0^{m/2} K(m_x, m - m_x) \cdot n(m_x) n(m - m_x) dm_x - n(m) \int_0^{\infty} K(m_x, m) \cdot n(m_x) dm_x \quad (1)$$

where $n(m)$ is the spectrum density of droplets, and K is the collection kernel between the two classes of droplets. The collection kernel describes the rate that droplets of mass m_x collected by $m - m_x$ and form new droplets of mass m . In Eq. (1), the first term describes formation of droplets of mass m through the collision of smaller droplets, and the second term means the loss of droplets of mass m through collision with other droplets. In order to solve SCE, it is necessary to get the collection kernel K . The collection kernel between droplets with mass m_1 and m_2 is

$$K(m_1, m_2) = |V_1 - V_2| \cdot \pi(r_1 + r_2)^2 \cdot E(m_1, m_2) \cdot \varepsilon \quad (2)$$

where V_1 and V_2 are the terminal velocity of each droplet, r_1 and r_2 are droplet radius, E is the collision efficiency, and ε is the coalescence efficiency. Obviously, $|V_1 - V_2| \cdot \pi(r_1 + r_2)^2$ means the geometric volume swept in unit time, but not all the small droplets in this volume could collide with large droplet. Because the flow induced by the larger droplet may drive some smaller droplets to flow past it. Thus, collision efficiency E is introduced as a proportion factor for true collision and it is much smaller than 1.0 when the droplet sizes are significantly different.



The physical meaning of E is shown in Fig. 1. The smaller droplet has smaller terminal velocity, so it moves upwards
65 relative to the larger droplet. Collision happens only when initial horizontal distance is smaller than threshold horizontal
distance r_c , or else the pair move apart. So, collision cross section is $S_c = \pi r_c^2$. Then collision efficiency is defined as $E =$
 $r_c^2/(r_1 + r_2)^2$. There are lots of previous researches on collision efficiency E , by both numerical simulations and chamber
experiments.

And ε is the coalescence efficiency, namely the coalescence probability when two droplets collide. In fact, two droplets do
70 not always coalesce when they collide with each. Instead, observations show that the pair can possibly rebound away in some
cases, because of an air film temporally trapped between the two surfaces. Especially for droplets with radius both larger than
100 μm , the “coalescence efficiency” is remarkably less than 1.0 (Beard and Ochs, 1984). The formula of coalescence
efficiency ε is used from Beard and Ochs (1984).

In this study, electric charges and fields are taken into consideration. Cloud spectrum has two parameters—droplets mass
75 m (or radius r) and electric charge q . So, SCE with the two parameters (m, q) is

$$\begin{aligned} \frac{\partial n(m, q, t)}{\partial t} = & \int_0^{m/2} \left[\int_{-\infty}^{+\infty} K(m_x, q_x; m - m_x, q - q_x) \cdot n(m_x, q_x) n(m - m_x, q - q_x) dq_x \right] dm_x \\ & - n(m, q) \int_0^{\infty} \left[\int_{-\infty}^{+\infty} K(m_x, q_x; m - m_x, q - q_x) \cdot n(m_x, q_x) dq_x \right] dm_x \end{aligned} \quad (3)$$

Bott (2000) proposed a method to solve SCE on two-parameter spectrum, which took droplet mass and also interior
80 aerosol mass into consideration. In this work, however, the problem is more complicated, since the electric charge could
affect the collection kernel, just like Khain et al. (2004).

3 Method for calculating the collision efficiency of charged droplets

85 3.1 Droplet motion equation

In order to get the collision efficiency, the motion equation of droplets is integrated to get the trajectories of droplets. Droplet
motion not only depends on gravity and flow drag, but also depends on the electric force between droplets.

The motion equations for a pair of droplets are shown below,

$$90 \quad \frac{d\mathbf{v}_1}{dt} = \mathbf{g} - C \frac{6\pi r_1 \eta}{m_1} (\mathbf{v}_1 - \mathbf{u}_2) + \frac{\mathbf{F}_{e1}}{m_1} \quad (4a)$$

$$\frac{d\mathbf{v}_2}{dt} = \mathbf{g} - C \frac{6\pi r_2 \eta}{m_2} (\mathbf{v}_2 - \mathbf{u}_1) + \frac{\mathbf{F}_{e2}}{m_2} \quad (4b)$$

where \mathbf{g} is the gravitational acceleration, \mathbf{v} is the velocity vector of each droplet relative to the earth, \mathbf{u} is the flow velocity
field induced by each droplet (also relative to earth), η is the fluid viscosity, and C is the drag coefficient, which is a function



of Reynolds number. Droplet mass $m = 4\pi r^3 \rho / 3$, and F_e is the electrostatic force caused by droplet electric charge and the
95 external vertical electric field. The fluid property is treated as air with temperature $T = 283$ K and pressure $p = 900$ hPa. The
three terms on the rhs is gravity, flow drag force, and electric force respectively.

3.2 The drag force term

100 The superposition method is used to solve the motion equation of droplets in a hydrodynamic flow, assuming that each droplet
moves in the flow field induced by the other one moving alone. This method has been successfully used in many researches
of collision efficiency calculation (Pruppacher and Klett, 1997).

Considering a sphere moving in a viscous fluid, the exact solution of the induced flow velocity field is to solve the Navier-
Stokes equations. However, the computation is too complicated in this study. An appropriate idea is that the stream function
105 depends on Reynolds number N_{Re} . Hamielec and Johnson (1962, 1963) gave the stream function ψ induced by a moving
rigid sphere:

$$\psi_h = \left(\frac{A_1}{R} + \frac{A_2}{R^2} + \frac{A_3}{R^3} + \frac{A_4}{R^4} \right) \sin^2 \theta - \left(\frac{B_1}{R} + \frac{B_2}{R^2} + \frac{B_3}{R^3} + \frac{B_4}{R^4} \right) \sin^2 \theta \cos \theta \quad (5)$$

where R is the distance from the sphere centre, θ is the angle between the vertical direction and vector \mathbf{R} pointing from the
sphere centre, and A_1, \dots, B_4 are functions of instant Reynolds number $N_{Re} = \frac{2rv\rho}{\mu}$ for each droplet. The method is valid for
110 $N_{Re} < 5000$. But the solution deviates from the Stokes flow solution when $N_{Re} \rightarrow 0$ for small droplets. Therefore, this work
adopts a smooth combination of ψ_h and Stokes stream function $\psi_s = v \left(\frac{R^3}{2r} - \frac{3rR}{2} \right) \sin^2 \theta$, (Pinsky and Khain, 2000)

$$\psi = \frac{N_{Re}\psi_h + N_{Re}^{-1}\psi_s}{N_{Re} + N_{Re}^{-1}} \quad (6)$$

which converges to stokes flow when $N_{Re} \rightarrow 0$. Then the induced flow field \mathbf{u} is derived,

$$\mathbf{u} = \frac{1}{R^2 \sin \theta} \frac{\partial \psi}{\partial \theta} \mathbf{e}_r + \frac{1}{R \sin \theta} \frac{\partial \psi}{\partial R} \mathbf{e}_\theta \quad (7)$$

115 The drag coefficient C is function of N_{Re} ,

$$C = 1 + \exp(a_0 + a_1 X + a_2 X^2) \quad (8)$$

where $X = \ln(N_{Re})$, and fitting constants a_0, a_1, a_2 are from table 2 of Beard (1976). The drag coefficient increases with
Reynolds number. For example, the terminal velocity of a droplet of $16 \mu\text{m}$ in radius is 3.12 cm s^{-1} , with $N_{Re} = 0.47$ and
 $C = 1.07$; the terminal velocity of a droplet of $1024 \mu\text{m}$ in radius is 7.15 m s^{-1} , with $N_{Re} = 777$ and $C = 21.3$. For $N_{Re} \rightarrow 0$, the
120 drag coefficient C is 1.

For droplets with $r < 10 \mu\text{m}$, the assumption of no-slip boundary condition is no longer valid. The flow slips on the
droplet surface. So, the drag coefficient should multiply another coefficient (Lamb and Verlinde 2011, p386)

$$C' = C \cdot \left(1 + 1.26 \frac{\lambda}{r} \right)^{-1} \quad (9)$$



where λ is the free path of air molecules, and r is the droplet radius.

125

3.3 The electric force term

It is well known that the interaction between two point charges can be expressed as

$$F_e = -\frac{q_1 q_2}{R^2} \quad (10)$$

130

However, this inverse-square law does not apply to uneven charge distribution, such as the case of charged cloud droplets.

The interaction between charged conductors is a complex mathematical physics problem. Davis (1964) demonstrated an appropriate computational method for electric force between two spherical conductors in an external uniform field, which depends on droplet radius (r_1, r_2), charge (q_1, q_2), centre distance R , electric field E_0 and angle θ between electric field and the line connecting the centres of two droplets. The electric force on droplet 2 with radius r_2 and charge q_2 is

135

$$\begin{aligned} \mathbf{F}_{e2} = \{ & r_2^2 E_0^2 (F_1 \cos^2 \theta + F_2 \sin^2 \theta) + E_0 \cos \theta (F_3 q_1 + F_4 q_2) + \frac{1}{r_2^2} (F_5 q_1^2 + F_6 q_1 q_2 + F_7 q_2^2) + E_0 q_2 \cos \theta \} \hat{\mathbf{e}}_R + \\ & \{ r_2^2 E_0^2 F_8 \sin 2\theta + E_0 \sin \theta (F_9 q_1 + F_{10} q_2) + E_0 q_2 \sin \theta \} \hat{\mathbf{e}}_\theta \end{aligned} \quad (11)$$

where $\hat{\mathbf{e}}_R$ is the radial unit vector, and $\hat{\mathbf{e}}_\theta$ is tangential unit vector. $F_1 \dots F_{10}$ are a series of complicated functions of geometric parameters (r_1, r_2, R ; Davis 1964).

140

Then, electric force on droplet 1 could be derived immediately by

$$\mathbf{F}_{e1} = E_0 (q_1 + q_2) \hat{\mathbf{e}}_z - \mathbf{F}_{e2} \quad (12)$$

145

The comparison between inverse-square law and conductor model are shown in Fig. 2, where the electric force of opposite charges (dashed lines) and of same charges (solid lines) varies with distance. It is shown that in remote distance, two models are basically identical. But when the spheres approach closely, the conductor interaction (blue lines) turns into strong attraction, because of electrostatic induction. It is significant that interaction must turn to attraction as long as the distance is small enough, regardless of sign of charge.

If there is only inverse-square law without electrostatic induction, it is obvious to say that same-sign charges must decrease collision efficiency. However, after taking electrostatic induction into account, the effects of same-sign and opposite-sign charges need to be reconsidered.

150

3.4 Droplet trajectory and the effective cross section

Eq. (4) is integrated to get the trajectories for the two droplets of any possible droplet pair (r_1, q_1 and r_2, q_2) in various strengths of downwards electric fields (0, 200 and 400 V cm⁻¹). The 2-order Runge-Kutta method is used for the integration.

155

Following their trajectories, the two droplets can either collide or not. In order to get the collision cross section $S_c = \pi r_c^2$ (or



say the collision efficiency E), we vary the initial horizontal distance between the two droplets using the bisection method, until we find a threshold distance r_c that makes the two droplets follow the grazing trajectories and just exactly collide. The threshold distance is found with a precision of 0.1%.

After the collision efficiency E is derived for droplet pair with (r_1, q_1) and (r_2, q_2) , the collection kernel $K(r_1, q_1, r_2, q_2)$ is derived, where the coalescence efficiency ε is restricted in the range from 0.3 to 1.0, using the formula of Beard and Ochs (1984). With the collection kernel $K(r_1, q_1, r_2, q_2)$, the effect of electric charges and fields on droplet collision is determined by the SCE.

4 Model setup for solving the stochastic collection equation

165

The evolution of the droplet spectrum is described by the 2-parameter SCE, i.e. Eq. (1). To solve the equation numerically, droplet radii and charges are divided into discrete logarithmically equidistant bins. Droplet radius ranging from 2 to 1024 μm is divided into 37 bins. The radius is increased by a factor of $2^{1/4}$ from one bin to the next. For droplet radius $r > 1024 \mu\text{m}$, they are assumed to precipitate out and not included in droplet spectrum.

170 Droplet charges are set to be proportional to the square of droplet radii, based on observations. Droplet charges ranging from $-32r^2$ to $+32r^2$ are divided into 15 bins, that is, $q = r^2 \times \{-32, -16, \dots, -0.5, 0, +0.5, +1, +2, \dots, +16, +32\}$. Under thunderstorm conditions, the amount of droplet charge is about $42r^2$ (in unit of elementary charge, and r in μm , converted from Pruppacher and Klett 1997). Therefore, the upper limit $32 r^2$ in this work approaches the thunderstorm condition.

Usually the droplet mass and charge after coalescence do not fall in any existing bins. A simple method is to linearly redistribute the droplets to the two neighbouring bins (Khain et al, 2004). We first redistribute droplets to the certain mass bins. The ratio of redistribution is based on total-mass conservation and droplet-number conservation simultaneously. For example, to redistribute droplets with mass m ($m_i < m < m_{i+1}$) and number Δn , a proportion of $\Delta n_i = \frac{m_{i+1}-m}{m_{i+1}-m_i} \Delta n$ is added

175 to the i th bin, and $\Delta n_{i+1} = \frac{m-m_i}{m_{i+1}-m_i} \Delta n$ is added to the $(i+1)$ th bin. After mass redistribution to the i th and $(i+1)$ th mass bins, the charge is redistributed within each of the mass bins, satisfying total-charge conservation and droplet-number conservation. For example, to redistribute droplets with charge q ($q_{i,j} < q < q_{i,j+1}$) within the i th mass bin, a proportion of $\Delta n_{i,j} = \frac{q_{i,j+1}-q}{q_{i,j+1}-q_{i,j}} \Delta n_i$ is added to the bin of (i, j) , and a proportion of $\Delta n_{i,j+1} = \frac{q-q_{i,j}}{q_{i,j+1}-q_{i,j}} \Delta n_i$ is added to the bin of $(i, j+1)$.

As shown in Fig. 3, the coalescence between bin (r_1, q_1) and bin (r_2, q_2) , shown with black dots, generates a droplet show with a red dot. This newly generated droplet is then redistributed into 4 bins shown with blue dots. Note that the numbers of each blue dot in Fig. 3 are the percentages in the redistribution of droplets to the bins. In fact, this method only reaches the first-order precision. Although Bott (1998) compared several methods to redistribute droplets with high-order correction, the two-parameter spectrum is too complicated to do the high-order correction in this study.

185 The initial droplet number density spectrum is assumed to be gamma distribution and adopted from Bott (1998),



$$n(m) = \frac{L}{\bar{m}^2} \exp\left(-\frac{m}{\bar{m}}\right) \quad (13)$$

where $L=1 \text{ g m}^{-3}$ is liquid water content, and \bar{m} is the mean droplet mass. The number density spectrum $n(m)$ can also multiply droplet mass, thus producing the mass spectrum,

$$M(m) = m \cdot n(m) = \frac{mL}{\bar{m}^2} \exp\left(-\frac{m}{\bar{m}}\right) \quad (14)$$

and can also be written as:

$$M(\ln r) = r^6 \frac{3L}{\bar{r}^6} \exp\left(-\frac{r^3}{\bar{r}^3}\right) \quad (15)$$

where \bar{r} is mean droplet radius (with $\bar{m} = 4\pi\bar{r}^3\rho/3$), which is an important variant to describe the cloud droplet size.

12 cases with different initial conditions are considered to study the spectrum evolution. The mean droplet radius \bar{r} is set by 3 different sizes: 15 μm , 9 μm and 6.5 μm , where $\bar{r} = 6.5 \mu\text{m}$ represents polluted conditions, and 15 μm case represents the clean conditions. For each \bar{r} , comparisons are made among 4 different electric conditions, including the uncharged cloud, charged cloud, charged cloud with a field of 200 V cm^{-1} , and charged cloud with a field of 400 V cm^{-1} (This study considers the downward electric fields as positive). For the uncharged cloud, the initial distribution is shown in Fig. 4a, where all droplets are put in the bins with no charge. For charged clouds, the initial charge is distributed symmetrically, as shown in Fig. 4b: 14% with charge $+1r^2$, 14% with charge $-1r^2$, 22% with charge $+0.5r^2$, 22% with charge $-0.5r^2$, and 28% with no charge (charge in unit of elementary charge, and r in μm), which represent the electric state in a normal precipitation process. During the computation of spectrum evolution, each bin could coalesce with any other bins in each step time Δt , which require the collection kernel between the two bins. Thus, a large matrix of kernel $K(r_1, r_2, q_1, q_2)$ is computed in advance. The initial electric charges, and electric field strength are set according to the conditions in the early stage of thunderstorms or warm clouds. In fact, in some extreme thunderstorm cases, both the electric charge and field could be one order of magnitude larger (Takahashi, 1973) than the values used in this study. Furthermore, in natural clouds, the electric charge on a droplets leaks away gradually. In this study, the charge leakage is assumed as a process of exponential decay (Pruppacher and Klett, 1997), and the relaxation time is set to $\tau = 120 \text{ min}$. Namely, all the bins lose $\frac{\Delta t}{\tau}$ of electric charge in each step time $\Delta t = 1 \text{ s}$.

5 Results

5.1 Collision efficiency

The collision efficiencies for droplets without electric charge or field are shown in Fig. 5. The radius of the larger droplet r_1 ranges from 30 to 305 μm . The coloured lines are computation results in this study, and the dots are from previous experiment results. It is clear that our results are basically consistent with those from previous studies. Collision efficiencies



220 increase with r_2 from 2 to 14 μm , and also increase with r_1 from 30 to 305 μm . For droplet pair that are both large enough, collision efficiencies are close to 1.

With the collision efficiencies of droplets with different radii and charges in different strength of electric fields all computed, it is found that the electric effect is sensitive to droplet radii. Results are only discussed for $r_1 = 30 \mu\text{m}$ and shown in Fig. 6. Totally 6 combinations of electric conditions are selected to be shown here, and the details are summarized in table
225 1. The droplet pair is set to have no charge, same-sign charges, or opposite charges. The electric field is set to be 0 or 400 V m^{-1} . Compared to the no-charge pair (curve 1), the same-sign charges without electric field (curve 2) slightly decreases collision efficiency, because of the repulsive force. The results of both positively charged pair and negatively charged pair are identical, since there is no electric field. In a downward electric field, the collision efficiency of the two situations is
230 that enhancement of electric field offset the repulsive effect. For a positively charged pair (curve 3), the collision efficiency is very close to the no-charge pair, which implies that enhancement of electric field offset the repulsive effect. For a negatively charged pair in a downward field (curve 4), the collision efficiency with small r_2 is significantly enhanced. This could be easily explained by electrostatic induction: the strong downward electric field induces positive charge on the lower part of the larger droplet (even though it is overall negatively-charged), so the smaller negative-charged droplet below feels attraction.

As for a pair with opposite charge, curve 5 shows that the collision efficiency is higher than the pair with no charge. For r_2
235 $< 5 \mu\text{m}$, the collision efficiency is nearly an order of magnitude higher; which for larger droplet the increase is not so strong. This means that the electric effect is sensitive to the radius of droplets, and mainly affects small droplets. Curve 6 shows that with an electric field of 400 V cm^{-1} , the electric effect becomes significantly stronger. Collision efficiency is increased by more than one order of magnitude compared to no-charge condition when $r_2 < 5 \mu\text{m}$. Even if r_2 is large, the collision efficiency could still be increased by about 2 times.

240

5.2. Evolution of cloud spectrum

This part shows the electric effect on spectrum evolution with different initial size distributions, i.e., $\bar{r} = 15 \mu\text{m}$, 9 μm and
245 6.5 μm . For each initial size distribution, comparisons are made among four different electric conditions, including uncharged, charged without field, charged with 200 V cm^{-1} and charged with 400 V cm^{-1} . Note that “charged” here refers to initial distribution shown in Fig. 4. The magnitude of 400 V cm^{-1} corresponds to the early stage of a thunderstorm.

Figure 7 shows the evolution of the spectrum with initial $\bar{r} = 15 \mu\text{m}$. The 4 rows show different times ($t = 7.5, 15, 22.5,$
and 30 min) during spectrum evolution. The left side denotes the spectrum mass density, and the right side shows the droplet
250 number concentration. In each panel, the dotted line denotes initial spectrum distribution ($t = 0 \text{ min}$) for reference. It is seen that droplet spectra under 4 electric conditions have similar behaviour. All the spectra evolve to a double-peak form, regardless of electric charge or field. At 30 min, the 4 cases all have a modal radius of about 200 μm (Fig. 7d). The electric



effect is not notable for large droplets, and the initial radius is large enough to start gravitational collision quickly.

Consequently, the electric effect is negligible in this case.

255 Figure 8 shows the evolution of the spectrum with initial $\bar{r} = 9 \mu\text{m}$. For the uncharged spectrum, it takes 60 min to have the second peak grow to about 200 μm . Therefore, the 4 panels of Fig. 8 show the spectrum evolution for $t = 15, 30, 45,$ and 60 min. The charges and the electric fields have more significant effect in the $\bar{r} = 9 \mu\text{m}$ case than in the $\bar{r} = 15 \mu\text{m}$ case. It is seen that, at 15 and 30 min, the spectra with different electric conditions evidently differ from each other, but the second mode is not obvious. At 45 min, the effect of charges and electric fields on the second peak is evident. The small-droplet
260 peak on the left is lower, and the second peak on the right is higher, indicating that the charged cloud (red line) evolves more quickly than the uncharged cloud. Moreover, vertical electric fields further boost the collision-coalescence process of charged droplets (green and purple lines). Under the electric field of 200 V cm^{-1} , the second peak is two times higher than the no-field case (red line) at 45 min. Under the electric field of 400 V cm^{-1} , the second peak is even higher. At 60 min, modal radius of second peak is about 200 μm for uncharge situation, 300 μm for charged without field situation, 500 μm for
265 charged with 200 V cm^{-1} situation, and 700 μm for charged with 400 V cm^{-1} situation, respectively.

The 2-dimensional spectrum for $\bar{r} = 9 \mu\text{m}$ at 60 min is shown in Fig. 9. Figure 9a is for the uncharged situation. Figures 9b, 9c, and 9d are for the situations with charges and with electric fields of 0, 200, 400 V cm^{-1} , respectively. After 60 min of evolution, these charge distributions are still nearly symmetric. These clearly show the process that charges transport to large droplets during coalescence growth. Note that the integration of this 2-dimensional spectrum along the charge axis gives the
270 size distribution at 60 min shown in Fig. 8d.

Figure 10 shows the evolution of the spectrum with initial $\bar{r} = 6.5 \mu\text{m}$. For the uncharged cloud, it takes 120 min to have the second peak grow to about 200 μm . Therefore, the 4 panels of Fig. 10 show the spectrum evolution for $t = 30, 60, 90$ and 120 min. The enhancement of the electric field on collision-coalescence process is much more obvious than $\bar{r} = 9 \mu\text{m}$. After 90 min of evolution, the spectra of the uncharged cloud (blue line) and charged cloud without field (red line) are almost the
275 same as the initial spectrum. This is because the droplets are too small to initiate gravitational collision. At 120 min, a second peak has formed for the situations with no charge and with charge but no field. In comparison, under the external electric field of 200 and 400 V cm^{-1} (green and purple lines), the cloud droplets grow much more quickly than the no-field situations. Some droplets even have evolved to larger than 1024 μm , which are supposed to precipitate out from the clouds. These results show that, the electric field would remarkably trigger the collision-coalescence process for the small droplets.

280 As for the initial mean droplet radius $\bar{r} < 6 \mu\text{m}$ (figure not shown), similar to Fig. 10, the spectra of uncharged and charged cloud without electric field would nearly have no difference, while the effect of electric fields is much stronger. This means that charge effect is relatively small compared to electric fields when the initial droplet radius of the cloud is small enough.

6 Discussion

285



According to Eq. (2), collection kernel K is composed of the collision efficiency E , relative terminal velocity, and coalescence efficiency ε . It is found that the total electric effect on K is mainly contributed by E . The electric enhancement of collision efficiency E is particularly significant for small droplets, as shown in Sect. 6.1. The relative terminal velocity term also contributes to the collection kernel, and the electric field can affect terminal velocity of small charged droplets significantly. As shown in Fig. 11, in downwards electric field 400 V cm^{-1} , terminal velocity of a large droplet is nearly not affected. The difference of velocity at $r = 1000 \mu\text{m}$ does not exceed 1%, and difference at $100 \mu\text{m}$ does not exceed 5%. On the contrary, electric fields strongly affect the sedimentation of charged small droplets. For $r < 5 \mu\text{m}$, the terminal velocity of negative-charged droplet even turns “upwards”. This is due to the fact that droplet mass $m \propto r^3$, while droplet charge $q \propto r^2$ according to observation. So, $q \propto m^{2/3}$ means that acceleration of electric force decreases with increasing droplet mass, which indicates that small droplets are more sensitive to electric charges and fields.

This study neglects some possible electric effects in collision-coalescence process. Electric effect on coalescence efficiency ε is neglected. Rebound (collide but not coalesce) happens because of an air film temporally trapped between the two surfaces, which is a barrier to coalescence. This barrier may be overcome by strong electric attraction occurring at small distance. Many experiments show that electric charges and fields would enhance coalescence efficiency, such as Jayaratne and Mason (1964). But there is no proper numerical model to evaluate the effect. So, this study may underestimate the electric effect on droplet collision-coalescence process.

Induced charge redistribution is also neglected when rebound happens. For instance, let us consider a rebound event in a positive (downwards) electric field. The larger droplet is often above the smaller droplet, and the smaller one will carry positive charge instantaneously according to electrostatic induction, then move apart. So, the rebound would cause charge redistribution between the pair. This may lead to some change in spectrum evolution.

7 Conclusion

The effect of electric charges and atmospheric electric fields on the evolution of cloud droplet spectrum is studied numerically. The motion equation of droplets in the atmosphere is solved to get the trajectories of droplet pair of any radii (2 to $1024 \mu\text{m}$) and charges (-32 to $+32r^2$, in unit of elementary charge, droplet radius r in unit of μm) in different strength of downwards electric fields (0, 200 and 400 V cm^{-1}). Based on trajectories, we determine whether a droplet pair collide or not. Thus, collision efficiencies for the droplet pairs are derived. It is seen that collision efficiency is increased by electric charges and fields, especially when the droplet pair are oppositely charged or both negatively charged in a downward electric field. The increase is particularly significant for a pair of small droplets.

With collision efficiencies derived in this study, SCE is solved to simulate the evolution of cloud droplet spectrum. The initial droplet size conditions include $\bar{r} = 15 \mu\text{m}$, $9 \mu\text{m}$, and $6.5 \mu\text{m}$, and the initial electric conditions include uncharged and charged (with charge amount proportional to droplet surface area) in different strength of electric fields (0, 200 and 400 V cm^{-1}). It is seen that the effects of both the electric charges and fields are not notable for the cloud with initial $\bar{r} = 15 \mu\text{m}$, since the



320 initial radius is large enough to start gravitational collision quickly. For the cloud with initial $\bar{r} = 9 \mu\text{m}$, electric charges could
enhance spectrum evolution evidently compared to the uncharged condition when there is no electric field, and the existence
of electric fields further accelerates large-drop formation. For the cloud with initial $\bar{r} = 6.5 \mu\text{m}$, it is difficult for gravitational
collision to occur. The enhancement of droplet collision merely by electric charge without field is still not significant, but
325 electric fields could remarkably enhance the collision process. These results indicate that the cloud with small droplet size is
more sensitive to electric charges and fields, which could significantly trigger the raindrop formation.

The magnitudes of electric charges and fields used in this study represent the real conditions in the atmosphere. In the natural
precipitation process, the charge amount, the strength of electric fields, and the time scale of droplet spectrum evolution are
similar to those in this study. It is known that the increase of aerosol number and therefore the decrease of cloud droplet size
lead to suppressed precipitation and longer cloud lifetime, as observed in the polluted clouds (Albrecht, 1989). But with the
330 existence of electric charges and fields, this Albrecht effect can be mitigated to a certain extent.

Code and data availability

Data and programs are available from Shian Guo (guoshian@pku.edu.cn) upon request.

335 Author contribution

Shian Guo developed the model, wrote the codes of program, and performed the simulation. Huiwen Xue advised on the
case settings of the numerical simulation. Huiwen Xue and Shian Guo worked together to prepare the manuscript.

Competing interests

340 The authors declare that they have no conflict of interest.

Acknowledgements

This study is supported by the National Innovative Training Program and the Chinese NSF grant 41675134. We are grateful
to Jost Heintzenberg and Shizuo Fu for constructive discussions on this study.

345

References

- Albrecht, B. A.: Aerosols, cloud microphysics, and fractional cloudiness., *Science*, 245, 1227–1230,
doi:10.1126/science.245.4923.1227., 1989
- 350 Beard, K. V.: Terminal velocity and shape of cloud and precipitation drops aloft, *J. Atmos. Sci*, 33, 851-864, doi:
10.1175/1520-0469(1976)033<0851:TVASOC>2.0.CO;2, 1976
- Beard, K.V. and Ochs III, H.T.: Collection and coalescence efficiencies for accretion, *J. Geophys. R.*, 41, 863-867,
doi:10.1029/JD089iD05p07165, 1984



- Bott, A.: A flux method for the numerical solution of the stochastic collection equation, *J. Atmos. Sci.*, 55, 2284-2293, doi: 10.1175/1520-0469(1998)055<2284:AFMFTN>2.0.CO;2, 1998
- 355 Bott, A.: A flux method for the numerical solution of the stochastic collection equation: extension to two-dimensional particle distributions, *J. Atmos. Sci.*, 57, 284-294, doi: 10.1175/1520-0469(2000)057<0284:AFMFTN>2.0.CO;2, 2000
- Davis, M. H.: Two charged spherical conductors in a uniform electric field: Forces and field strength, *Q. J. Mech. Appl. Math.*, 17, 499– 511., doi:10.1093/qjmam/17.4.499, 1964
- 360 Hamielec, A. E. and Johnson, A. I.: Viscous flow around fluid spheres at intermediate Reynolds numbers, *Can. J. Chem. Eng.*, 40, 41-45, doi:10.1002/cjce. 5450400202, 1962
- Hamielec, A. E. and Johnson, A. I.: Viscous flow around fluid spheres at intermediate Reynolds numbers (II), *Can. J. Chem. Eng.*, 41, 246-251, doi:10.1002/cjce.5450410604, 1963
- Jayarathne, O. W. and Mason, B. J.: The coalescence and bouncing of water drops at an air/water interface, *P. R. Soc. London*, 365 280, 545-565, doi:10.1098/rspa.1964.0161, 1964
- Khain, A., Arkhipov, V., Pinsky, M., Feldman, Y. and Ryabov., Ya.: Rain enhancement and fog elimination by seeding with charged droplets. part I: theory and numerical simulations. *J. Appl. Meteorol.*, 43:1513–1529, doi:10.1175/JAM2131.1, 2004.
- Lamb, D. and Verlinde, J.: *Physics and Chemistry of Clouds*, Cambridge University Press, 2011
- Pinsky, M., and Khain, A.: Collision efficiency of drops in a wide range of Reynolds numbers: effects of pressure on spectrum evolution, *J. Atmos. Sci.*, 58, 742-763, doi: 10.1175/1520-0469(2001)058<0742:CEODIA>2.0.CO;2, 2000
- 370 Pruppacher, H. R. and Klett, J. D.: *Microphysics of Clouds and Precipitation*, Kluwer Academic Publishers, 1997
- Schlamp, R. J., Grover, S. N., Pruppacher, H. R., and Hamielec, A. E.: A numerical investigation of the effect of electric charges and vertical external electric fields on the collision efficiency of cloud drops, *J. Atmos. Sci.*, 33. 1747-1755, doi:10.1175/1520-0469(1976)033<1747:ANIOTE>2.0.CO;2, 1976
- 375 Takahashi, T.: Measurement of electric charge of cloud droplets, drizzle, and raindrops, *Rev. Geophys. Space. Ge.*, 11, 903-924, doi:10.1029/RG011i004p00903, 1973
- Telford, J. W.: A new aspect of coalescence theory, *J. Meteorol.*, 12, 436-444, 1955

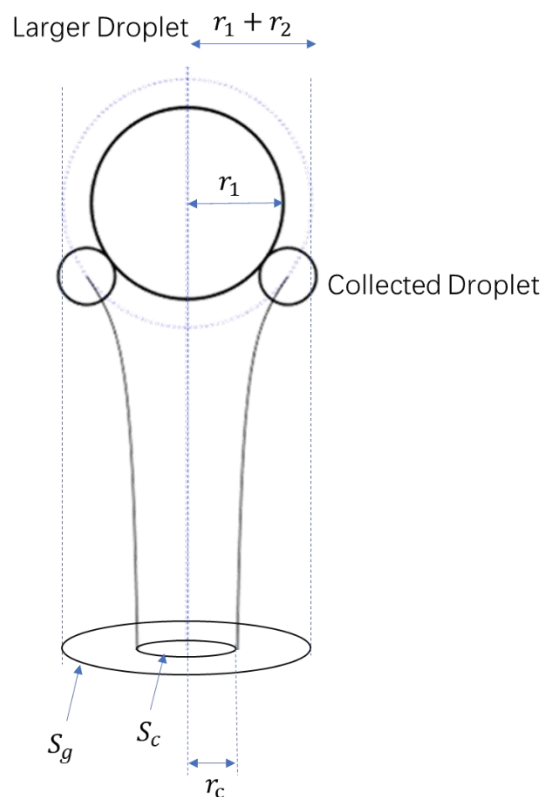


380

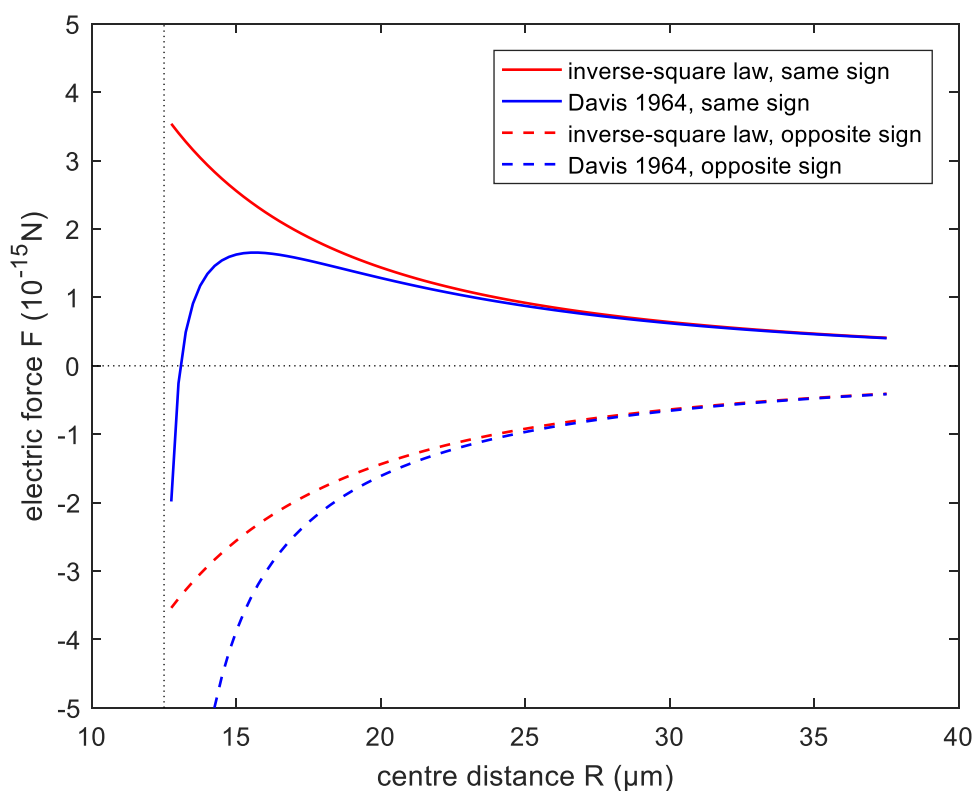
Table 1. Meaning of the 6 different curves in Fig. 6.

settings	q_1 (e)	q_2 (e)	electric field E_0 (V cm ⁻¹)
(1)	0	0	0
(2)	+32 r_1^2	+32 r_2^2	0
(3)	+32 r_1^2	+32 r_2^2	+400
(4)	-32 r_1^2	-32 r_2^2	+400
(5)	+32 r_1^2	-32 r_2^2	0
(6)	+32 r_1^2	-32 r_2^2	+400

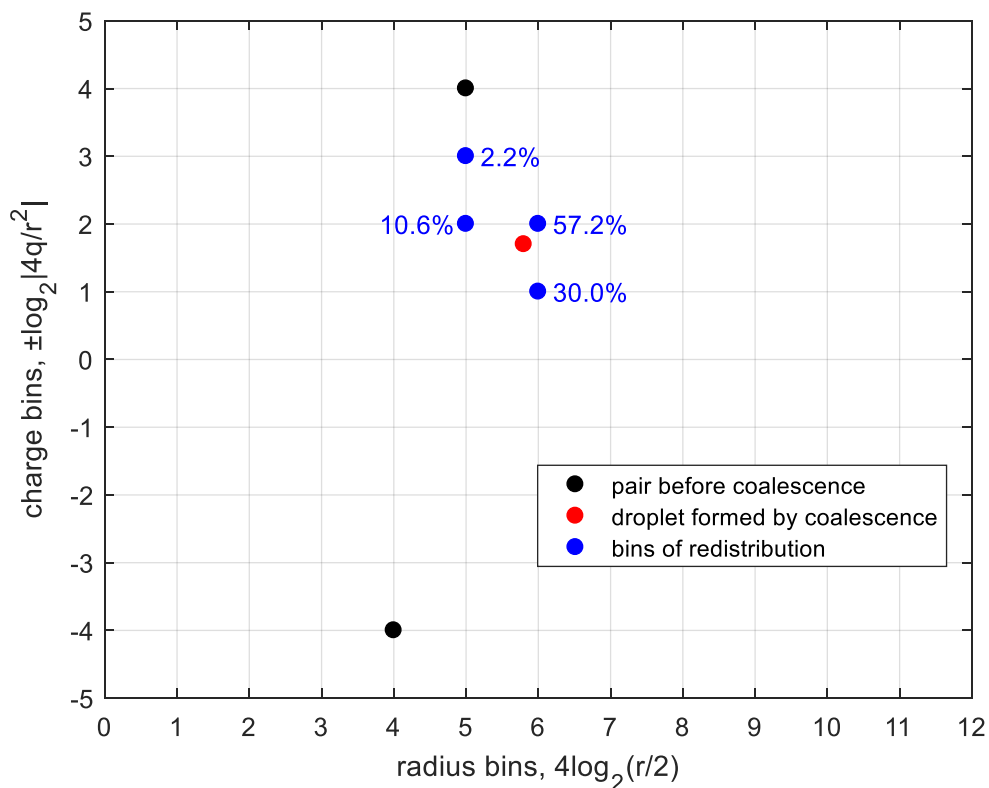
385



390 **FIG. 1.** A geometry sketch map of collision. Original vertical distance is set to $\Delta y_0 = 30(r_1 + r_2)$, which approximates to coming from infinity. To calculate the collection section $S_c = \pi r_c^2$, we need to adjust the initial horizontal distance by bisection method, until it converges to r_c . Collision happens only when the initial horizontal distance is smaller than r_c .



395 **FIG. 2.** Comparison between electric force of conductor model and inverse-square law, where positive represents repulsion and negative represents attraction. Radius of the pair is set to $r_1 = 10 \mu\text{m}$ and $r_2 = 2.5 \mu\text{m}$ respectively, and dashed lines denote opposite sign of electric charge: $q_1 = +100 e$, $q_2 = -25 e$; solid lines denote the same sign of electric charge: $q_1 = +100 e$, $q_2 = +25 e$.



400

FIG. 3. An example of redistribution of coalescence between two bins. Black dots denote the two bins of droplets before coalescence. The red dot refers to the droplet after coalescence but not on the bin grids. The blue dots show the redistribution method and proportion of each redistributed bin, which is constrained by particle-number conservation, mass conservation and charge conservation.

405

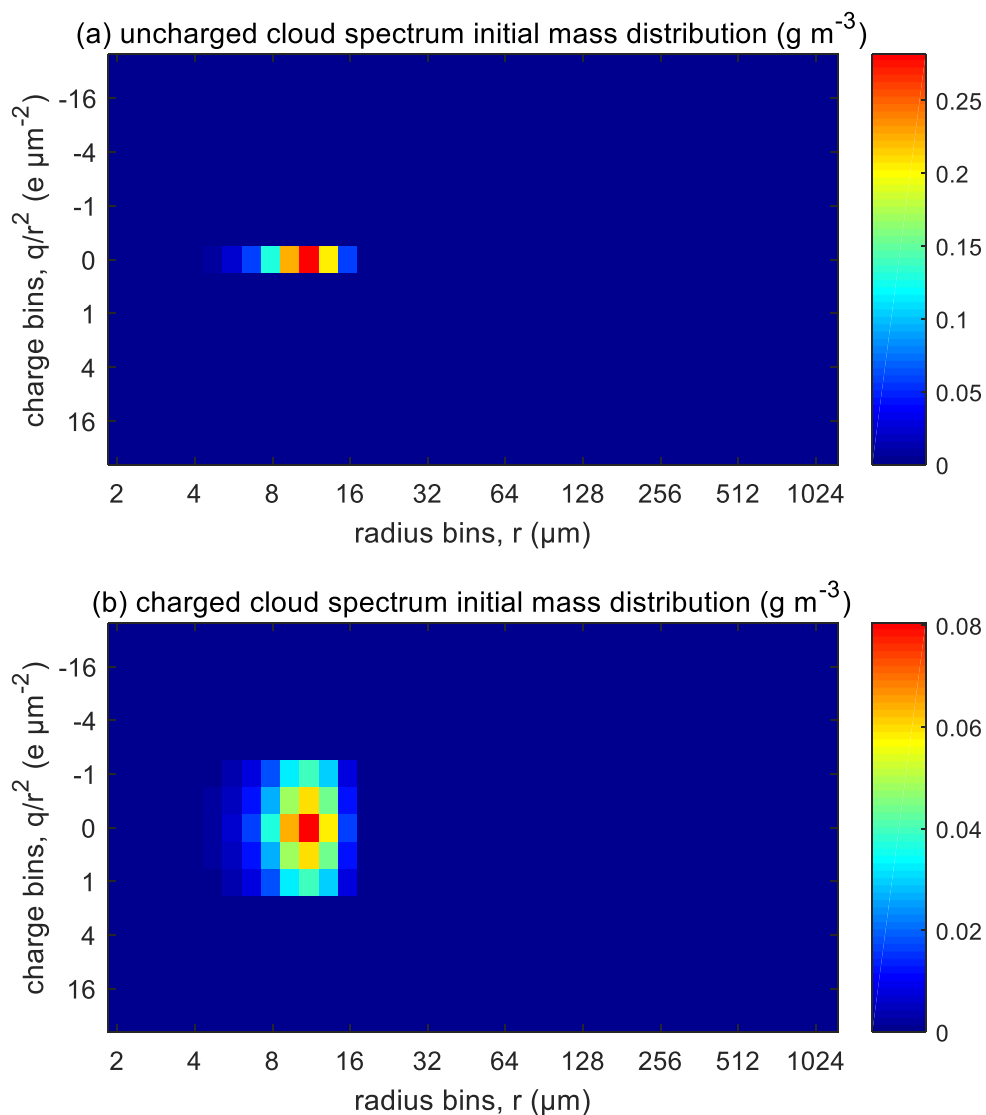
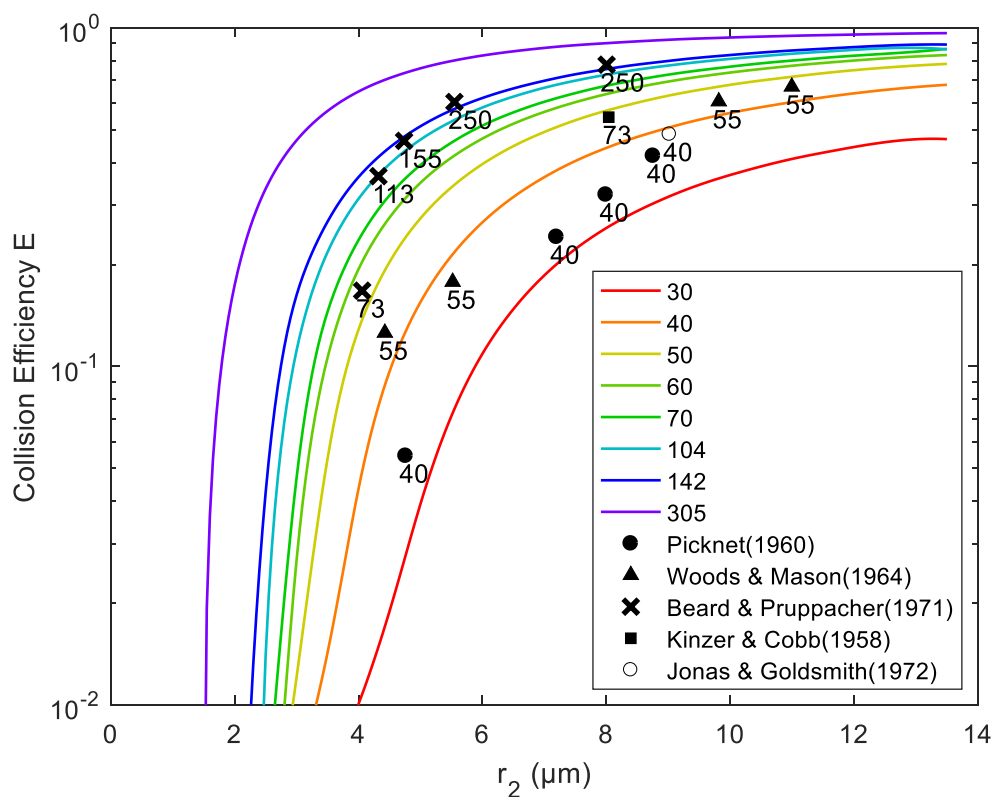
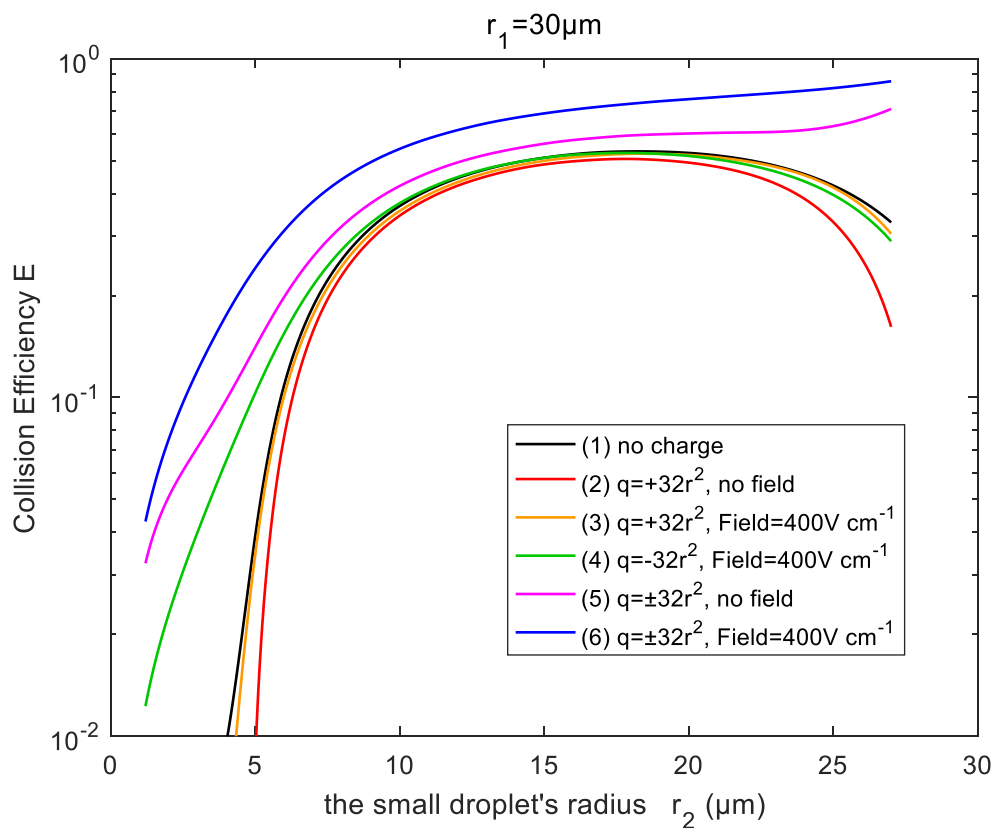


FIG. 4. Initial spectrum mass distribution shown in 2-dimensional grids of bins. Different colours stand for water mass content in these bins (g m^{-3}). (a) Uncharged spectrum mass distribution (b) charged spectrum mass distribution.



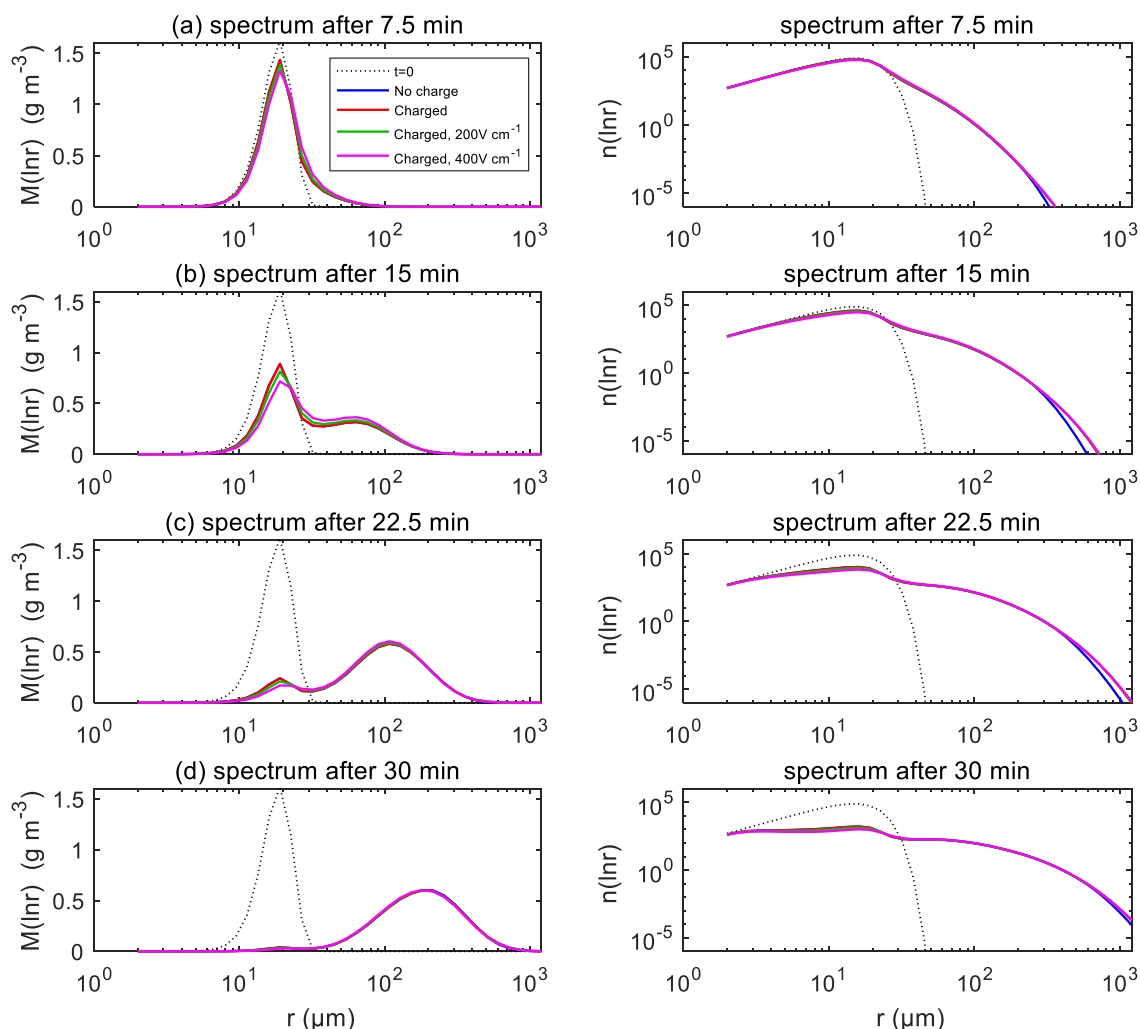
410

FIG. 5. Collision efficiency between droplets without electric charge. Colour lines are results computed in this study. Different curves show different the large droplet radius r_1 , from 30 to 305 μm . X-axis denotes the smaller droplet radius r_2 , and Y-axis denotes collision efficiency with different large droplets. Scatter points are from previous experimental studies.



415

FIG. 6. Collision efficiency in different electric conditions. The radius of the larger droplet $r_1 = 30.0 \mu\text{m}$. X-axis denotes the radius of the smaller droplet r_2 , and Y-axis denotes collision efficiency in different electric conditions. The two droplets carry opposite charge (proportional to r^2).



420

FIG. 7. The evolution of the spectrum with initial $\bar{r} = 15 \mu\text{m}$. These panels show different stages of spectrum evolution from top to bottom. The left side shows the mass density of cloud spectra, and the right side show the number concentration of droplets under logarithmic coordinates. In each panel, comparisons are made by 4 different electric conditions. Blue lines denote the uncharged cloud spectrum. Red lines denote charged cloud without electric field. Green and purple lines denote charged cloud with field 200 V cm^{-1} and 400 V cm^{-1} , respectively. Dotted lines show the initial mass distribution.

425

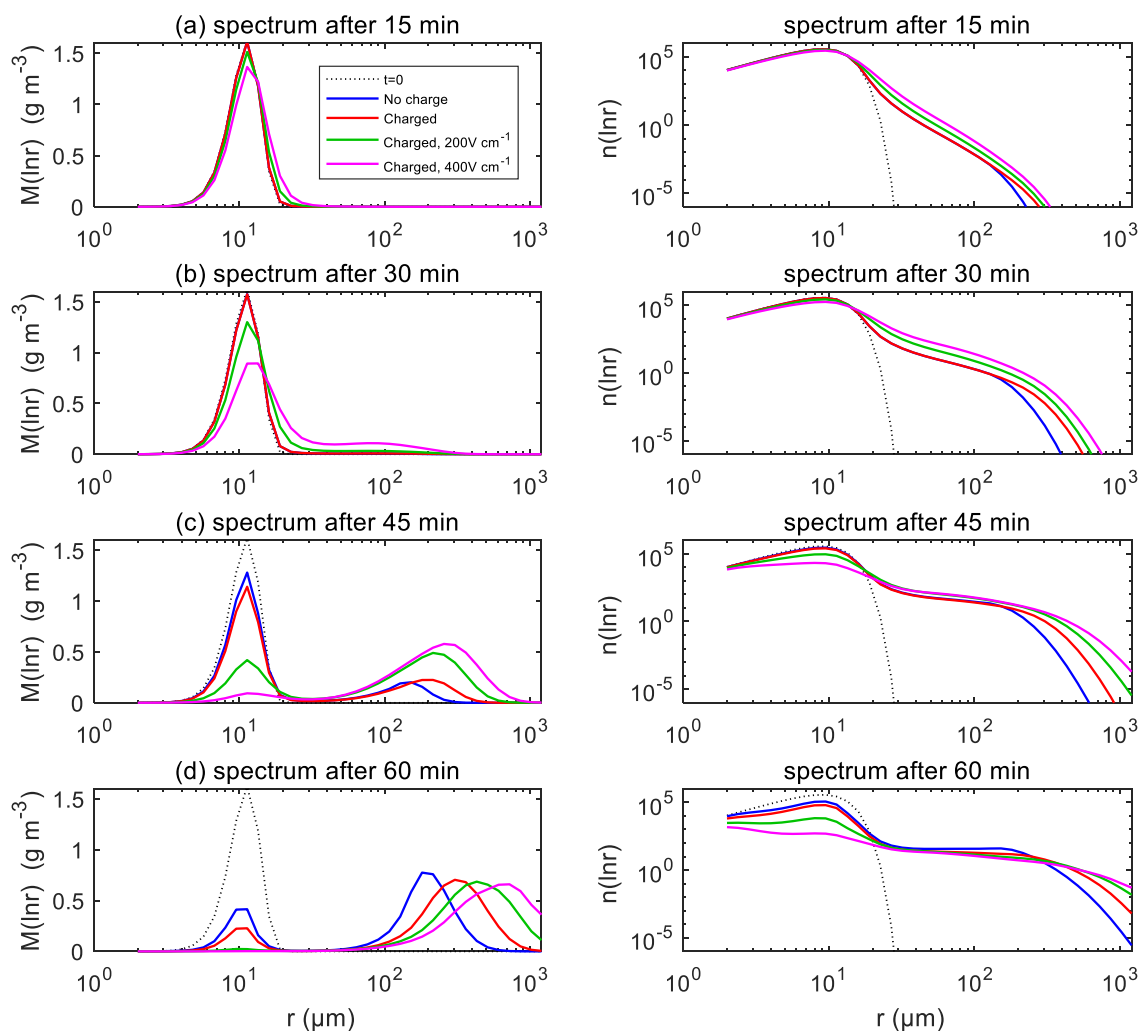
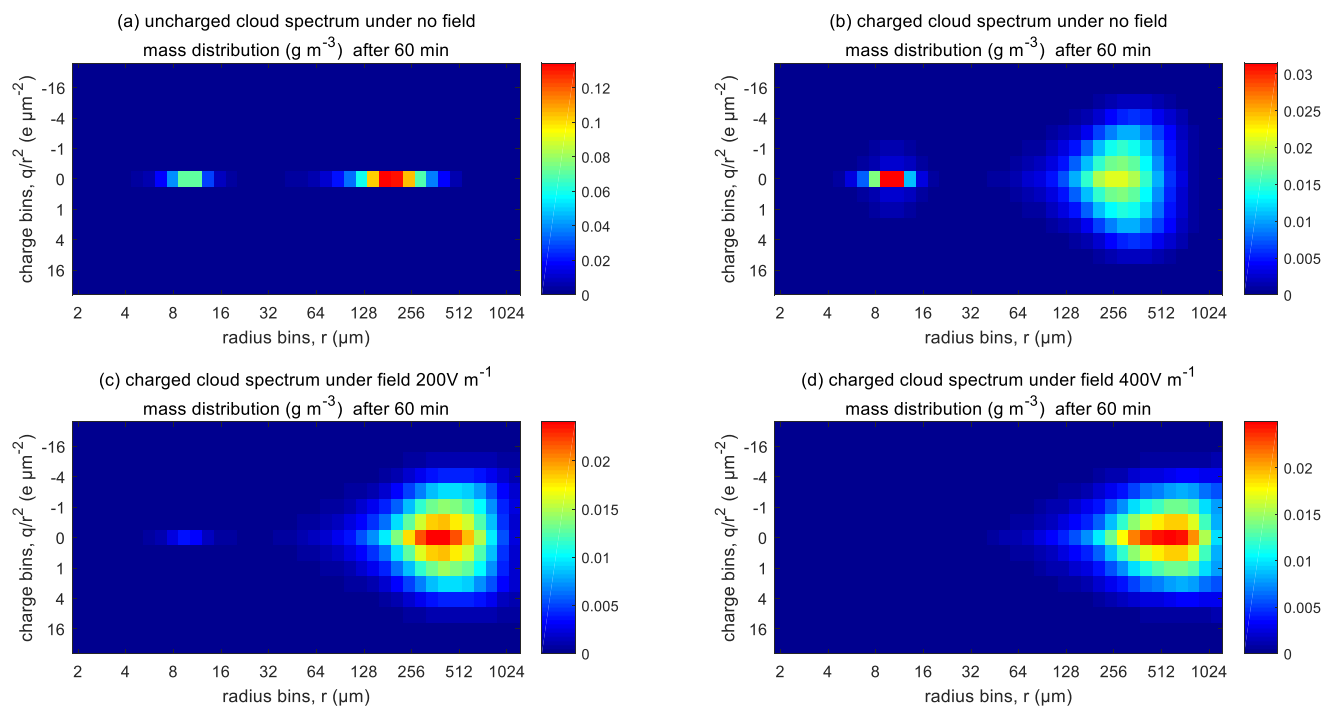


FIG. 8. The evolution of the spectrum with initial $\bar{r} = 9 \mu\text{m}$.



430

FIG. 9. Comparison of 2-dimensional spectrum evolution with different electric conditions at 60 min (initial $\bar{r} = 9 \mu\text{m}$).

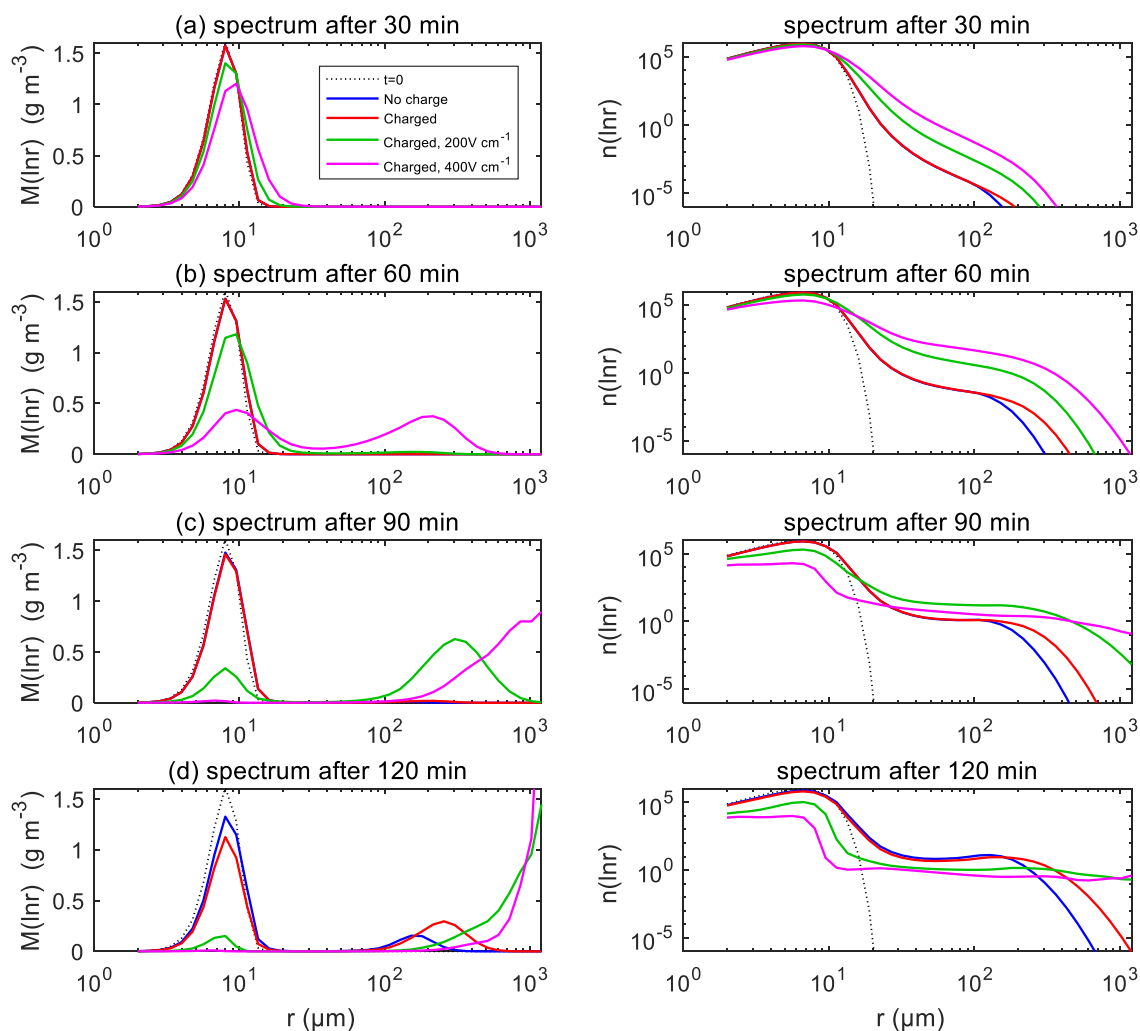


FIG. 10. The evolution of the spectrum with initial $\bar{r} = 6.5 \mu\text{m}$.

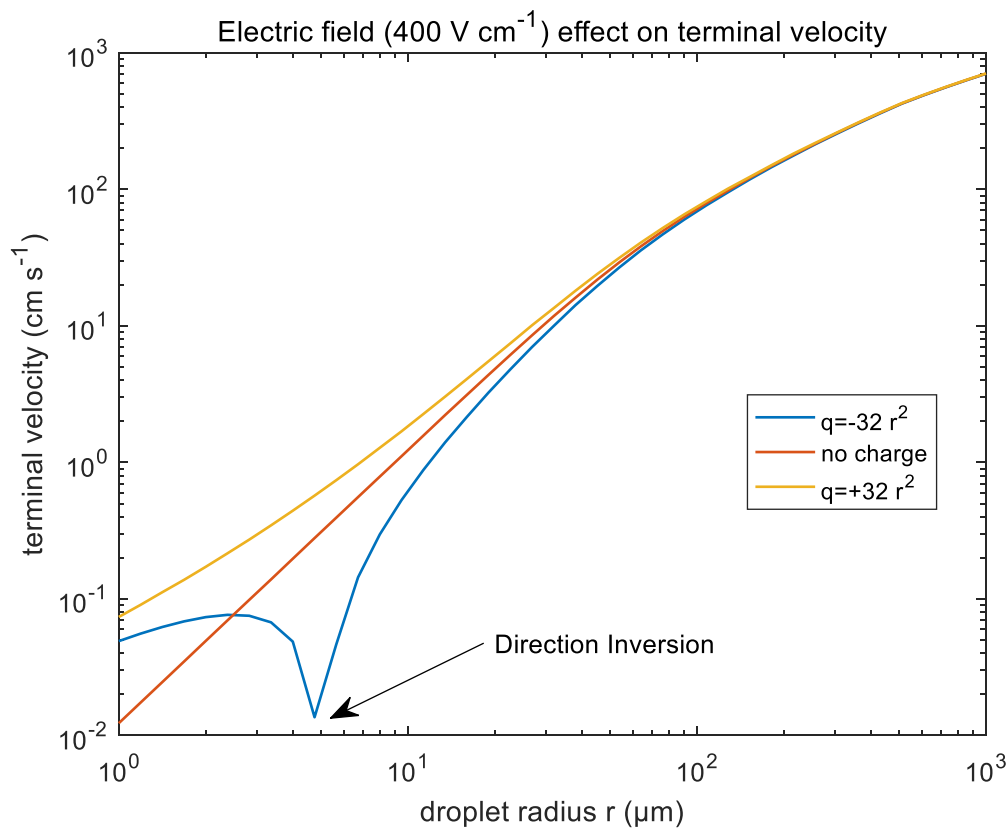


FIG. 11. Terminal velocities of droplets in external electric field 400 V cm⁻¹. Different lines denote different droplet charge conditions. It is significant that terminal velocity of negatively charged droplets smaller than 5 μm would turn upwards, which leads to the discontinuity of the lower curve in the figure.